

Local Residual Error Estimators for the Method of Moments Solution of Electromagnetic Integral Equations

Usman Saeed and Andrew F. Peterson

School of Electrical and Computer Engineering
Georgia Institute of Technology
Atlanta, GA, 30332-0250, USA
Email: usaeed@gatech.edu, peterson@ece.gatech.edu

Abstract — Several methods for estimating the local (cell-by-cell) error associated with a method of moments solution of the electric field integral equation are investigated. Three different residual error estimators are used with a variety of prototype structures. The global error estimates show reasonable correlation with the actual current density errors, and all three local error estimators correctly identify the high-error regions. Utility of the proposed error estimators is presented through a simple h -refinement technique.

Index Terms — Adaptive refinement, boundary element method, method of moments, residual error.

I. INTRODUCTION

Electromagnetic field problems often involve the prediction of fields in the presence of complicated structures, and the solution of these problems usually rests upon computational procedures. Integral equation formulations have been widespread, and are discussed in several texts [1-3]. The typical numerical solution process involves creating a subsectional mesh model for the surface of any structures, representing the equivalent surface currents on that surface by a piecewise-polynomial basis, and imposing boundary conditions on the fields to construct a large linear system of equations. The solution of that system produces the coefficients of those polynomial basis functions. That process is known as the *method of moments* or the *boundary element method*. Although the numerical treatment of integral equations has steadily advanced for

decades, adaptive refinement procedures have lagged behind other developments. Adaptive refinement is an approach where either (a) the mesh density, or (b) the polynomial degree employed in certain regions of the mesh, is automatically modified as required to improve the accuracy of the approach, without user intervention. Such modification must be based on an estimate of the local error [4-11].

In the present study, we consider the transverse-electric (TE)-to- z electric field integral equation (EFIE) for two-dimensional conducting structures. The continuous equation being solved can be expressed as

$$\bar{L} \{ \bar{J} \}_{\tan} = \bar{g}_{\tan}, \quad (1)$$

where \bar{J} , the electric current density, is the quantity of interest, and

$$\bar{L} \{ \bar{J} \} = \frac{1}{j\omega\epsilon} \{ \nabla \nabla \bullet + k^2 \} \quad (2)$$

$$\int \bar{J}(t') \frac{1}{4j} H_0^{(2)}(k|\bar{r} - \bar{r}'|) dt',$$

$$\bar{g} = -\bar{E}^{inc}(\bar{r}), \quad (3)$$

where \bar{E}^{inc} is the given excitation, $H_0^{(2)}$ is the zero-order Hankel function of the second kind, t and t' denote parametric variables along the contour of the structure, and \bar{r} is the position vector from t' to t on the contour.

The numerical solution for the current density is obtained in terms of a representation in N basis functions

$$\bar{J}_N(t) = \sum_{n=1}^N J_n \bar{B}_n(t). \quad (4)$$

The surface of the conducting scatterer is represented by flat facets, while the current density is represented by an expansion using piecewise-linear or “triangle” basis functions $\{\bar{B}_n(t)\}$ that are tangential to the surface. Each triangle function straddles two of the facets in the surface model. A weighted-residual approach is employed using piecewise-constant or pulse testing functions $\{\bar{T}_m(t)\}$, also tangential to the surface and partially straddling adjacent cells, to construct a system of equations that may be expressed in matrix form as

$$ZJ = E. \quad (5)$$

The entries of the N by N system matrix and the N by 1 excitation vector are given by

$$Z_{mn} = \int \bar{T}_m \cdot \bar{L} \{\bar{B}_n\} dt, \quad (6)$$

$$E_m = \int \bar{T}_m \cdot \bar{g} dt. \quad (7)$$

Other details of the numerical solution procedure, including approximations that were used in the computation of Z_{mn} , are described in section 2.4 of [3].

Local error estimators are often based on residual error computations. Once the coefficients in (2) have been determined, the tangential residual associated with this numerical result can be written as

$$R_{\tan}(t) = \bar{L} \{\bar{J}_N\}_{\tan} - \bar{g}_{\tan}. \quad (8)$$

The residual error is known to correlate with the actual error $\bar{e} = \bar{J} - \bar{J}_N$ [12], and has formed the basis for determining solution error in various integral equation formulations [13-14]. However, it is relatively expensive to compute, since it usually must be evaluated using an approach that is independent from that used to construct the original linear system.

In the following, we consider several different error estimators related to (8), and compare their performance and computational efficiency on a number of canonical scattering targets.

II. TANGENTIAL RESIDUAL ERROR ESTIMATOR

The TE EFIE imposes the tangential-field boundary condition

$$E_{\tan}^{tot} = 0, \quad (9)$$

indirectly, by equating the average value of the residual in (8) over the domain of the testing function to zero. In other words, in the construction of the linear system in (5), equation (9) is imposed in an average sense by integrating it with a piecewise-constant testing function from the center of one cell to the center of the adjacent cell. In the preceding notation, this is equivalent to imposing

$$\int R_{\tan}(t) dt = 0, \quad (10)$$

over the domain of each pulse testing function.

The residual in (10) provides a means to measure the error in a particular result, and is directly computable since it does not depend directly on the exact solution. However, if we compute the residual error in the same manner as was used to construct the linear system in (5), we do not obtain useful information since the equations are exactly satisfied. However, we could re-compute the residual error in a variety of ways to obtain an independent measure of the residual error.

Consider the use of weighting functions that are centered within each cell with their widths made relatively small (1/5 of the cell width in this case). In that case, the residual error at the center of cell i may be obtained as

$$R_i(t_i) = \int_{\text{small domain at center of cell } i} R_{\tan}(t) dt, \quad (11)$$

where R_{\tan} is computed from the previously-obtained numerical values for the current density, using essentially the same subroutines as used to compute the matrix entries Z_{mn} .

The normalized tangential residual error in the i^{th} cell may be defined as

$$TR_i^{loc} = \frac{|R_i(t_i)|}{|\bar{g}|_{\max}}, \quad (12)$$

to provide a local measure of the error. In (12), $|\bar{g}|_{\max}$ denotes the maximum magnitude of the excitation (3) used in the residual calculation of (11). For a global measure of the error, we employ the 2-norm error obtained by summing (12) over all the cells in the model:

$$TR_2^{glo} = \sqrt{\frac{1}{N} \sum_{i=1}^N (TR_i^{loc})^2}. \quad (13)$$

As a consequence of the definition of the residual in (11), these error measures are relatively independent of the system of equations that led to the specific numerical solution being evaluated.

III. NORMAL RESIDUAL ERROR ESTIMATOR

In the preceding section, a residual error estimator was constructed based on enforcing the tangential field boundary condition. An additional boundary condition should be satisfied by the normal component of the total electric field at the surface of a perfect conductor, namely

$$\hat{n} \bullet \bar{E}^{tot} = \frac{\rho_s}{\varepsilon}, \quad (14)$$

where ρ_s denotes the surface charge density at a point on the surface, ε denotes the permittivity of the exterior medium, and \hat{n} is an outward-directed unit vector perpendicular to the surface. The boundary condition of (14) may be expressed in the form of an alternative residual

$$N(t) = \hat{n}(t) \bullet \left(\bar{L} \{ \bar{J}_N \} - \bar{g} \right) + \frac{1}{j\omega\varepsilon} \frac{d\{\hat{t}(t) \bullet \bar{J}_N\}}{dt}, \quad (15)$$

which uses

$$\rho_s = -\frac{\nabla_s \bullet \bar{J}_N}{j\omega} = -\frac{1}{j\omega} \frac{d\{\hat{t}(t) \bullet \bar{J}_N\}}{dt}. \quad (16)$$

For ease of computation and employing the same subroutines used to build the matrix in (5), we orient the testing functions so that they are now normal to the cells, at the cell center, and compute the normal residual in the i^{th} cell using

$$NR_i^{loc} = \frac{1}{|\bar{g}|_{\max}} \int_{\text{perpendicular to cell } i} N(t) dn, \quad (17)$$

where the testing domain is typically on the order of the cell size, and $|\bar{g}|_{\max}$ denotes the maximum magnitude of the excitation used in the residual calculation of (15). The global error NR_2^{glo} is obtained in the same manner as equation (13).

IV. ERROR ESTIMATION BASED ON AN OVER-DETERMINED SYSTEM OF EQUATIONS

A third way to compute a residual is to set up and solve an overdetermined system of equations

representing (1), by employing more testing functions (over smaller domains) than basis functions when constructing equation (5) [13-15]. A least-squares approach can be used to obtain a solution that minimizes the error in the residual equations. Since the equations will not be exactly satisfied, the residual can be computed from the equations and used directly as a measure of the error in the numerical result [14].

We use an implementation where the cells are divided in half, each with a tangential testing function centrally located, to yield a $2N$ by N system

$$\mathbf{Z}_{2N \times N} \mathbf{J}_N = \mathbf{E}_{2N}. \quad (18)$$

Unlike [13], these equations are equally weighted. After the current coefficients are determined by a least-square solution, the residual function is computed as the matrix column vector

$$R_{OD}(t_i) = \mathbf{Z}_{2N \times N} \mathbf{J}_N - \mathbf{E}_{2N}^{inc}. \quad (19)$$

The normalized tangential residual error at location i may be defined as

$$ODR_i^{loc} = \frac{|R_{OD}(t_i)|}{|E_{2N}^{inc}|_{\max}}. \quad (20)$$

A global function is obtained by summing over the $2N$ locations in accordance with (13). We note that one could alternatively mix tangential and normal testing functions.

V. SIMULATION RESULTS

In the following, we compare the performance of the preceding three error estimators on several geometries. We also estimate the actual error in each numerical result by comparison to a numerical result obtained with a finer discretization of the target. A local value for the normalized error in the i -th cell is obtained as

$$NE_i^{loc} = \frac{|\bar{J}_{ref}(t_i) - \bar{J}_N(t_i)|}{\max |\bar{J}_{ref}(t_i)|}, \quad (21)$$

with the global estimate obtained following (13).

Figure 1a shows the geometry of the first problem, which is a circular cylinder of 5λ circumference illuminated with two line sources placed (as shown) a distance of 0.1λ from the cylinder surface. For one of the line sources, the expression used for the incident E-field is given by

$$\bar{E}^{inc} = j\eta 2\pi H_1^{(2)}(k\rho) \left[\hat{x} \frac{y-y'}{\rho} - \hat{y} \frac{x-\hat{x}}{\rho} \right]. \quad (22)$$

The region of the cylinder that is nearer to the line sources ($\varphi = 180^\circ$) is expected to have more error in a typical numerical result for current density than the regions far away, since the current is more rapidly varying there. This is also observed, for example, in antennas near their feed region (and often motivates a higher discretization density in that region). Figure 1b shows the performance of the three residual-based error estimators for cylinder of figure 1a modeled with 200 cells. The reference solution in this case is the result obtained with 400 cells, and all three estimators predict a similar error pattern as the reference. All the estimators correctly identify the highest error region near $\varphi = 180^\circ$.

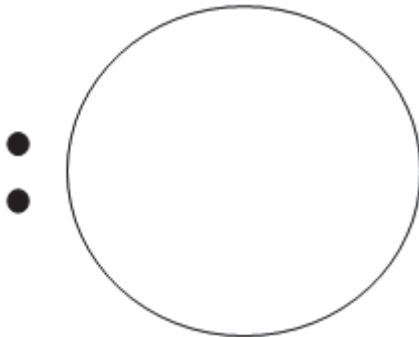


Fig. 1a. Geometry of the problem.

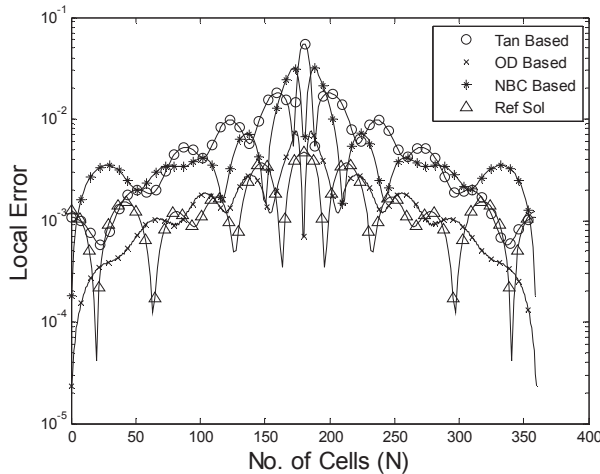


Fig. 1b. Local error for the problem of Figure 1a.

Figure 1c shows a plot of the global error produced by the same estimators, as a function of the number of unknowns or cells used in the computations. The global residual error levels decrease at approximately an $O(h)$ rate as the cylinder model is refined. As discussed below, this is different from the rate at which the actual

current density error decreases. These rates agree with those observed in [14–15] for the TE EFIE and linear basis functions.

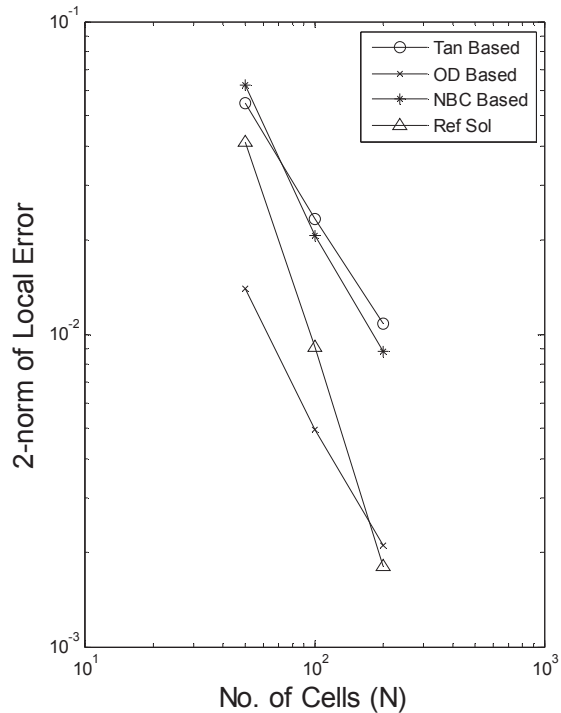


Fig. 1c. Global error for the problem of Figure 1a.

Figure 2a shows a keyhole-shaped cylinder, consisting of sections of two circular cylinders connected by a region with parallel walls. Figure 2b compares the performance of the three residual-based error estimators for a keyhole-shaped cylinder of 4.15λ total perimeter, modeled with 300 cells, for the same double line source excitation used in Figure 1. The larger end of the target has a radius of 0.32λ , while the smaller end has a radius of 0.14λ . The circular segments have centers separated by 1.32λ . The reference solution is obtained using 600 cells. There is a relatively large error level near the junction where the large circle meets the planar region (at 90° and 270°), and a larger error where the smaller circle meets the planar region (near 10° and 350°). The expected higher-error region at $\varphi = 180^\circ$ is correctly identified by the three estimators. Figure 2c shows a plot of the global error, as the number of unknowns used in the computations is varied. The global residual error levels decrease at approximately an $O(h)$ rate as the cylinder model is refined.

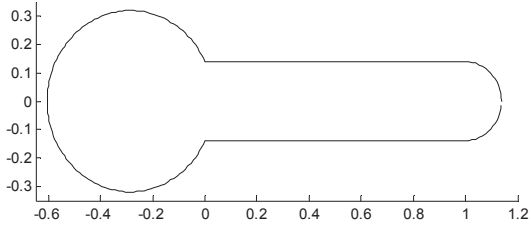


Fig. 2a. Geometry of the problem.

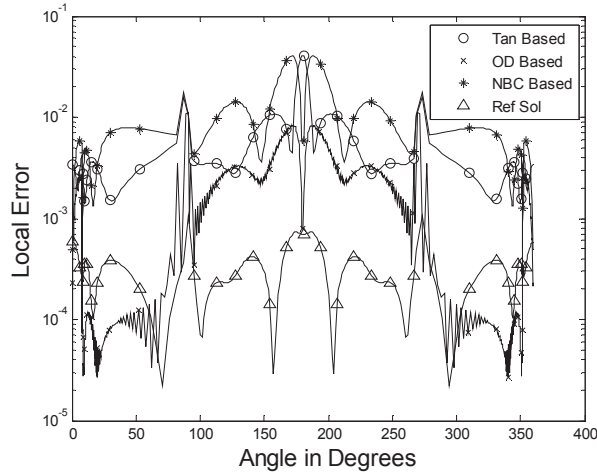


Fig. 2b. Local error for the problem of Figure 2a.

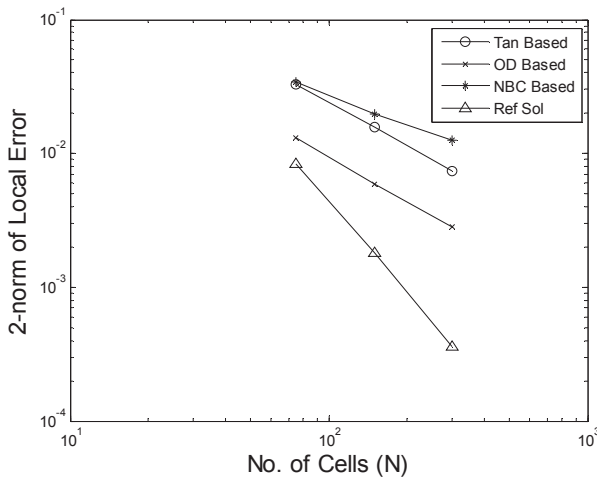


Fig. 2c. Global error for the problem of Figure 2a.

Figure 3 shows the local error computed by the three estimators for the same keyhole-shaped cylinder as shown previously in Figure 2a, but with a uniform plane wave excitation instead of line sources. The plane wave impinges symmetrically upon the larger end of the scatterer. It is expected that the error will be uniform except near discontinuities in the surface, as is confirmed by Figure 3. Error peaks near 10° and 90° angles

correspond to curvature discontinuities where the circular regions meet the planar region of the surface. The higher spike corresponds to the sharper corner. Another interesting observation is that the error level gradually rolls off with increasing distance from the corner cells. The global error behavior is similar to that shown in Figure 2c and is not repeated here.

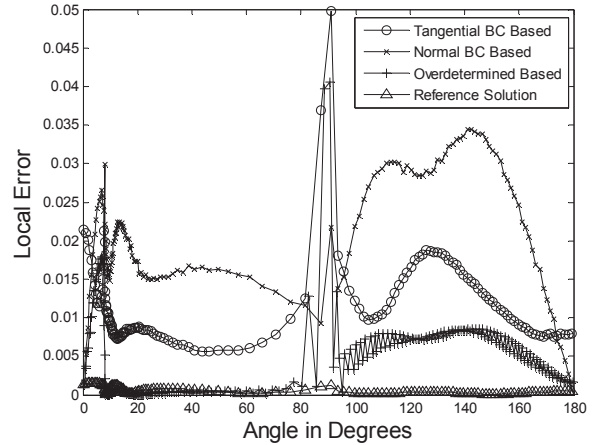


Fig. 3. Local error for the problem of Figure 2a for plane wave illumination.

VI. *h*-REFINEMENT

In this section, we demonstrate the utility of the tangential residual estimator presented in Section II to carry out adaptive *h*-refinement. This approach requires the cell size to be adaptively adjusted to control the error. The details of our *h*-refinement scheme are as follows. First, an initial coarse solution for the current density J is computed. That solution is used to compute the local error using the tangential residual error estimator. Once the local error values have been computed, they are sorted in descending order to identify the cells with the largest error levels. The 20% of those cells with the largest error are each divided into 3 cells, while each of the next 20% are divided into two cells. The remaining cells are left at their original size. After re-meshing, the problem is solved again to obtain a new solution for J , and a new local error estimate is obtained from the residual error. If the local error is still high or does not meet the user's criteria, the above procedure may be repeated recursively.

We implemented one iteration of the above procedure for a 5λ circumference cylinder illuminated with a pair of line sources as shown in

Figure 1a. The initial coarse solution was calculated for 100 cells and local error was computed. Based on the estimated local error values, a new mesh was created according to above scheme and is shown in Figure 4. The local error estimate computed before and after the adaptive refinement step is shown in Figure 5.

The tangential residual estimator identified the region of largest error to be that near the line source excitation, as expected, and the h -refinement step results in a large reduction of the tangential residual error in the refined region of the problem. Figure 6 shows the actual error in J , both before and after the adaptive refinement step, using (21) with a 600-cell solution for J as a reference.

Figure 6 shows that the error in J is reduced by a factor of more than 3 in the refined regions. After only one step of adaptive refinement, the combination of the tangential residual estimator and the h -refinement procedure produces a more uniform error level across the problem domain than originally obtained with a uniform mesh.

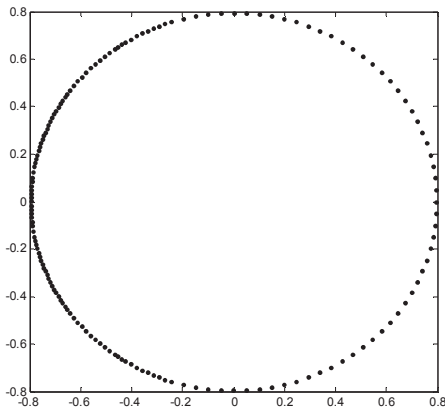


Fig. 4. Mesh density after the refinement.

VII. COMMENT ON THE GLOBAL ERROR RATES

In practice, the error in moment method results is usually dominated by the ability of the basis functions to represent the actual current density. For a piecewise-linear representation of a smoother function, this error should decrease at an $O(h^2)$ rate, where h is the nominal mesh size [3]. The reference solution error plotted in Figures 1c and 2c appears to decrease at approximately that rate. It has been observed in [14-15], and in Figures 1c and 2c, that for the TE EFIE operator,

the residual error decreases at a rate that is one order less, an $O(h)$ rate. This is apparently due to the TE EFIE operator, which contains one integral and two derivatives. We note that for the transverse-magnetic (TM) polarization, where the operator involves one integration and no derivatives, the EFIE residual error appears to decrease at a rate that is one degree faster than the current error. It appears that each integral increases the rate by one order while each derivative decreases the rate by one order, relative to that of the current density. It has been observed that the residual error associated with the magnetic field integral equation (MFIE) decreases at the same rate as the current density error [14-15], while error in far field quantities may decrease at different rates from the current density for all these integral operators [14].

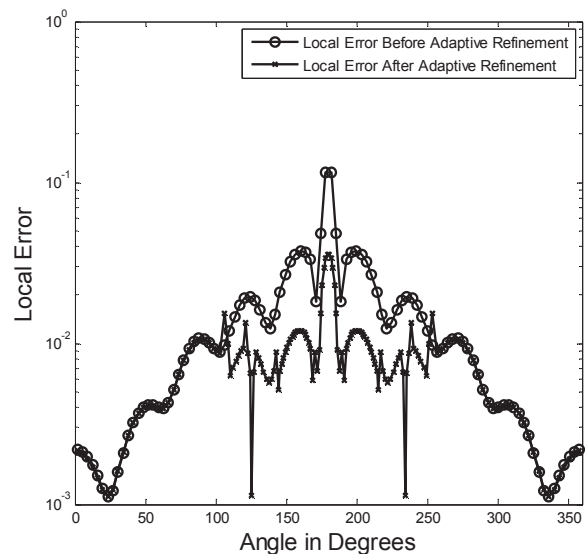


Fig. 5: Local error estimate before and after h -refinement.

The different error rates may limit our ability to use residual error estimators to determine the absolute global level of current density error in a particular result. Additional research is needed to address that issue. Despite this limitation, the residual estimators appear to be able to provide a local error distribution suitable for an adaptive refinement algorithm.

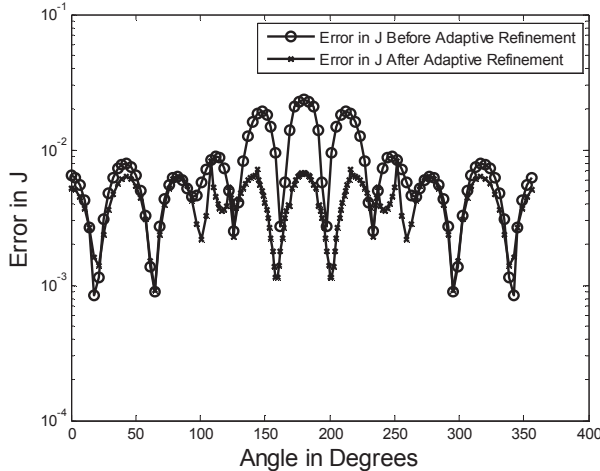


Fig. 6. Error in J before and after h -refinement.

VIII. COMPUTATIONAL COST OF ESTIMATORS

The relative computational cost of the estimators can be estimated as follows. The baseline cost without error estimation is

$$C_0 \cong \alpha N^2 + \beta N^3, \quad (23)$$

where α and β are the constants associated with matrix fill and solve times, respectively. The tangential and normal estimators add an approximate cost of

$$C_t \cong C_n \cong \alpha N^2, \quad (24)$$

since the residual computation in each case is comparable to an additional matrix fill.

The overdetermined error estimator has an approximate cost of

$$C_{over} \cong 2\alpha N^2 + 5\beta N^3, \quad (25)$$

since the matrix has twice as many entries, and since the least-square solution of a 2:1 rectangular system is reported to require about 5 times the operations of the LU factorization of a square system [16].

Thus, all three estimators add a cost of αN^2 operations, but the overdetermined estimator requires an additional $4\beta N^3$ operations beyond that. Thus, the overdetermined estimator is more expensive than the others, especially for large N .

IX. CONCLUSION

Three residual-based error estimators were considered for providing a local error estimate in conjunction with the method of moments solution of electromagnetic integral equations. All three

estimators successfully located higher-error regions in test problems. All appear to be suitable for use in adaptive refinement schemes. The tangential residual and normal residual estimators have comparable cost and generally gave comparable results. The overdetermined estimator also gave similar results, but requires additional computation compared to the others. An example employing h -refinement was presented for illustration.

It was noted that for the EFIE the residual error decreases at a different rate than the current density error as a function of the nominal cell size. At the present time, this limits the use of simple residual error estimators for predicting the absolute error associated with a particular result. Additional research is warranted to better understand the behavior of the various errors and determine more cost-effective ways of estimating those errors.

REFERENCES

- [1] R. F. Harrington, *Field Computation by Moment Methods*. New York: IEEE Press, 1993.
- [2] J. J. H. Wang, *Generalized Moment Methods in Electromagnetics – Formulation and Solution of Integral Equations*. New York: Wiley, 1991.
- [3] A. F. Peterson, S. L. Ray, and R. Mittra, *Computational Methods for Electromagnetics*. New York: IEEE Press, 1998.
- [4] F. J. C. Meyer and D. B. Davidson, “A Posteriori Error Estimates for Two-Dimensional Electromagnetic Field Computations: Boundary Elements and Finite Elements,” *Applied Computational Electromagnetic Society (ACES) Journal*, vol. 11, pp. 40-54, July 1996.
- [5] J. Wang and J. P. Webb, “Hierarchical Vector Boundary Elements and Adaptation for 3-D Electromagnetic Scattering,” *IEEE Trans. Antennas Propagat.*, vol. 45, pp. 1869-1879, December 1997.
- [6] M. Ainsworth and J. T. Oden, *A Posteriori Error Estimation in Finite Element Analysis*. New York: Wiley, 2000.
- [7] E. Kita and N. Kamiya, “Error Estimation and Adaptive Mesh Refinement in Boundary Element Method, an Overview,” *Engineering*

- Analysis with Boundary Elements*, vol. 25, pp. 479-495, 2001.
- [8] X. Wang, M. M. Botha, and J.-M. Jin, "An Error Estimator for the Moment Method in Electromagnetic Scattering," *Microwave and Optical Technology Letters*, vol. 44, pp. 320-326, February 2005.
- [9] M. M. Botha and D. B. Davidson, "An Explicit a Posteriori Error Indicator for Electromagnetic, Finite Element-Boundary Integral Analysis," *IEEE Trans. Antennas Propagat.*, vol. 53, pp. 3717-3725, November 2005.
- [10] M. M. Botha and D. B. Davidson, "Investigation of an Explicit, Residual-Based, A Posteriori Error Indicator for the Adaptive Finite Element Analysis of Waveguide Structures," *Applied Computational Electromagnetic Society (ACES) Journal*, vol. 21, no. 1, pp. 63-71, March 2006.
- [11] A. P. C. Fourie, D. C. Nitch, and A. R. Clark, "Predicting MoM Error Currents by Inverse Application of Residual E-Fields," *Applied Computational Electromagnetic Society (ACES) Journal*, vol. 14, no. 3, pp. 72-75, November 1999.
- [12] G. C. Hsiao and R. E. Kleinman, "Error Control in Numerical Solution of Boundary Integral Equations," *Applied Computational Electromagnetics Society (ACES) Journal*, vol. 11, pp. 32-36, 1996.
- [13] K. J. Bunch and R. W. Grow, "The Boundary Residual Method for Three-Dimensional Homogeneous Field Problems with Boundaries of Arbitrary Geometries," *International Journal of Infrared and Millimeter Waves*, vol. 10, pp. 1007-1032, 1989.
- [14] M. M. Bibby and A. F. Peterson, "On the Use of Over-Determined Systems in the Adaptive Numerical Solution of Integral Equations," *IEEE Trans. Antennas Propagat.*, vol. 53, pp. 2267-2273, July 2005.
- [15] M. M. Bibby, A. F. Peterson, and C. M. Coldwell, "High Order Representations for Singular Currents at Corners," *IEEE Trans. Antennas Propagat.*, vol. 56, pp. 2277-2287, August 2008.
- [16] G. H. Golub and C. F. Van Loan, *Matrix Computations*. Baltimore: Johns Hopkins University Press, 1989.



Usman Saeed received the B.Sc. and M.Sc. degrees in Electrical Engineering from the University of Engineering & Technology, Lahore, in 2004 and 2006, respectively. From 2004 through 2006, he was a Lecturer with the

Department of Electrical Engineering at the University of Engineering & Technology, Lahore. In 2006, he joined the Georgia Institute of Technology, Atlanta, GA as a Fulbright Fellow for M.S. studies. In 2008, he received the M.S. degree in Electrical and Computer Engineering from the Georgia Institute of Technology where he is currently working towards the Ph.D. degree.



Andrew F. Peterson received the B.S., M.S., and Ph.D. degrees in Electrical Engineering from the University of Illinois, Urbana-Champaign in 1982, 1983, and 1986 respectively. Since 1989, he has been a member of the faculty of the School of Electrical and Computer Engineering at the Georgia Institute of Technology, where he is now Professor and Associate Chair for Faculty Development. Within ACES, he served for six years as a member of the Board of Directors, and has been the Finance Committee Chair and the Publications Committee Chair. He was elevated to ACES Fellow in 2008. He served as a technical co-chair for the 25th Annual Review of Progress in Applied Computational Electromagnetics (ACES 2009) and is currently the ACES President.